

Local Off-Grid Weather Forecasting with Multi-Modal Earth Observation Data

Qidong Yang¹, Jonathan Giezendanner¹, Daniel Salles Civitarese², Johannes Jakubik², Eric Schmitt³, Anirban Chandra³, Jeremy Vila³, Detlef Hohl³, Chris Hill¹, Campbell Watson², and Sherrie Wang¹

¹Massachusetts Institute of Technology

²IBM Research

³Shell Information Technology International Inc.

Key Points:

- There is a systematic bias between gridded numerical weather products and off-grid local weather station measurements.
- A model combining gridded numerical weather products and off-grid weather measurements can make accurate and localized weather forecasts.
- Transformer is one of the best performing models for off-grid local weather forecasting due to its flexible attention mechanism.

Abstract

Urgent applications like wildfire management and renewable energy generation require precise, localized weather forecasts near the Earth’s surface. However, forecasts produced by machine learning models or numerical weather prediction systems are typically generated on large-scale regular grids, where direct downscaling fails to capture fine-grained, near-surface weather patterns. In this work, we propose a multi-modal transformer model trained end-to-end to downscale gridded forecasts to off-grid locations of interest. Our model directly combines local historical weather observations (e.g., wind, temperature, dewpoint) with gridded forecasts to produce locally accurate predictions at various lead times. Multiple data modalities are collected and concatenated at station-level locations, treated as a token at each station. Using self-attention, the token corresponding to the target location aggregates information from its neighboring tokens. Experiments using weather stations across the Northeastern United States show that our model outperforms a range of data-driven and non-data-driven off-grid forecasting methods. They also reveal that direct input of station data provides a phase shift in local weather forecasting accuracy, reducing the prediction error by up to 80% compared to pure gridded data based models. This approach demonstrates how to bridge the gap between large-scale weather models and locally accurate forecasts to support high-stakes, location-sensitive decision-making.

Plain Language Summary

In our research, we developed a new AI approach to make weather forecasts more accurate for specific locations, which is vital for urgent needs like wildfire management and renewable energy production. Traditional weather forecasts work on large grids covering wide areas. This makes them less reliable for specific spots on the ground where precise predictions matter most. Our method uses a special type of AI (a multi-modal transformer) that learns from both traditional forecasts and actual weather measurements from local weather stations. By combining these different data sources, our AI can "correct" the large-scale forecasts for specific locations. For example, our system looks at historical temperature, wind, and moisture readings from a network of weather stations, then uses this local knowledge to refine predictions for exact spots people care about. Our AI also cleverly considers how nearby weather stations relate to each other, giving more weight to stations that provide relevant information. When we tested our approach across the Northeastern United States, it provided more accurate local forecasts than existing methods. This improvement could help decision-makers in high-stakes situations like planning for wildfire response or managing renewable energy systems, where knowing precise local weather conditions can make a critical difference.

1 Introduction

In recent years, machine learning (ML) has been widely used in weather forecasting applications. This popularity stems from its fast inference speed and ability to model complex physical dynamics directly from data. Some high-profile ML weather forecasting models include FourCastNet (Pathak et al., 2022), GraphCast (Lam et al., 2023), and Pangu-Weather (Bi et al., 2023). These ML weather models can generate forecasts thousands of times faster than traditional numerical weather prediction (NWP) models, while at the same time being more accurate and flexible, freed from the NWP model’s sometimes restrictive physical constraints (Pathak et al., 2022; Lam et al., 2023; Kochkov et al., 2024).

To date, most ML weather models have been trained with gridded numerical weather reanalysis products like ERA5 (Hersbach et al., 2020). However, reanalysis products have been shown to have a systematic bias relative to the weather station measurements (Ramavajjala & Mitra, 2023). Here, we verify the existence of a substantial bias in ERA5’s near-surface

wind estimates (Figures 1 and 2). ERA5 systematically overestimates the inland near-surface wind speed and is much smoother across space than the actual wind field as measured by weather stations. ML models trained to predict numerical weather reanalysis inherit this significant bias and are unable to make accurate localized predictions.

This presents a challenge, as accurate off-grid weather forecasts are critical for applications like wildfire management and sustainable energy generation. To bridge this gap, we explore ML models to forecast localized weather patterns. These models digest multi-modal Earth observation data, including gridded numerical weather forecast products and local weather station measurements, to make accurate forecasts at irregularly spaced off-grid points.

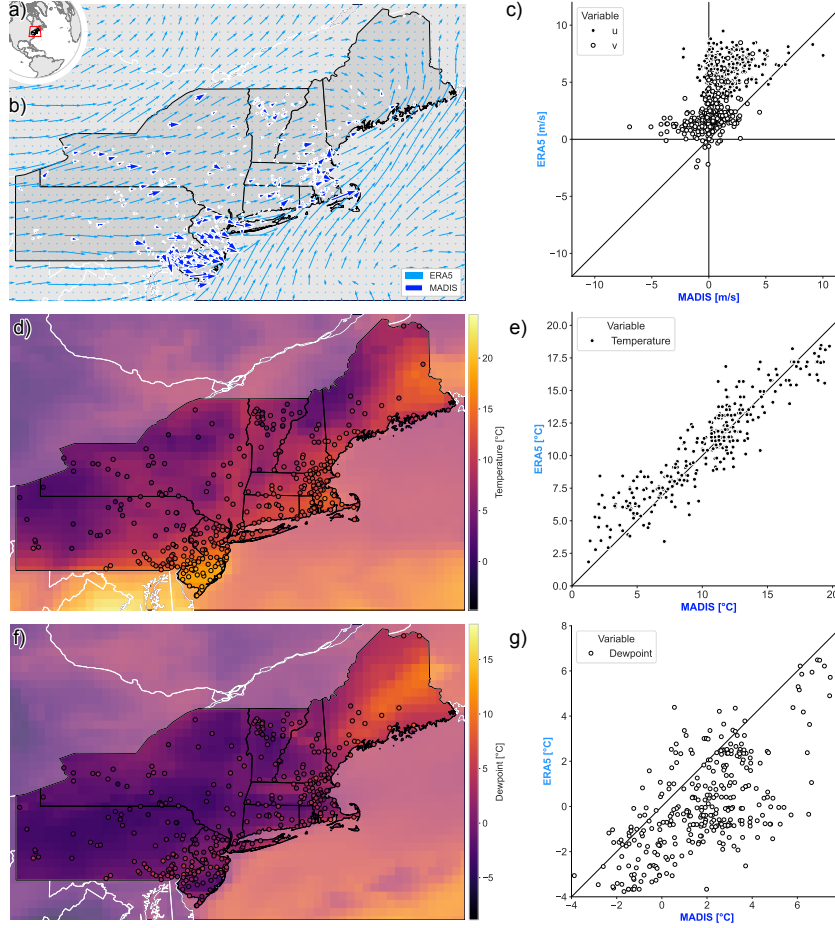


Figure 1. Gridded reanalysis data like ERA5 do not capture localized, near-surface weather dynamics. (a) Our study area is the Northeastern United States. (b) Wind field for April 18th, 2023 18:00–19:00, with ERA5 global reanalysis data in light blue and wind measured by weather stations (MADIS) in dark blue. (c) Scatterplot of MADIS vs. ERA5 for the same time, separated into u ($\rho^2 = 0.07$) and v ($\rho^2 = 0.12$) components of wind. The ERA5 data is linearly interpolated to the locations of the MADIS weather stations. (d) and (e) are the same plots for temperature ($\rho^2 = 0.85$). (f) and (g) show dewpoint ($\rho^2 = 0.46$).

First, we curate a dataset that contains both numerical weather products (ERA5 and HRRR) and local weather station observations (MADIS), spanning 2019–2023 and

covering the Northeastern United States. On top of the dataset, a transformer model is trained to make forecasts at each weather station. It tokenizes the weather measurements at each station and concatenates them with numerical weather estimates at nearby grid points. It processes the multi-modal input tokens with a stack of transformer encoder blocks, then makes a final prediction at each station by decoding the output of the last encoder block with a prediction head. As a competitive baseline, we also explore a graph neural network (GNN) to forecast at each weather station, as GNNs are widely used in multi-modal off-grid settings (Brandstetter et al., 2023) and in weather forecasting (Lam et al., 2023). Here, the GNN is built on a heterogeneous graph, where NWP grid points and off-grid weather stations are treated as two different types of nodes. The GNN operates on this graph and makes forecasts at each weather station. When making predictions at a station location, the GNN aggregates information from neighboring weather stations and numerical weather grid points using message passing (Gilmer et al., 2017).

These two methods preserve the irregular geometry of the off-grid stations and theoretically infinite spatial resolution, and ingest both gridded NWP and local weather station measurements. As a result, the prediction is informed by both large-scale atmospheric dynamics and local weather patterns. We evaluate our models’ ability to forecast real data from weather stations, focusing on temperature, dewpoint, and wind. Our transformer model outperforms a variety of other off-grid forecasting methods, including ERA5 interpolation and time series forecasting without spatial context. It also outperforms the GNN model by a significant margin, indicating that the transformer model is able to better capture the complex spatial relationships between weather stations.

Our contributions can be summarized as the following:

1. We compile and release a multi-modal weather dataset incorporating both off-grid MADIS weather stations and gridded ERA5 and HRRR. The dataset covers the Northeastern US from 2019–2023 and includes a comprehensive list of weather variables.
2. We verify, using our dataset, the systematic bias between gridded numerical weather products (ERA5 and HRRR) and off-grid local weather station measurements (MADIS).
3. We propose a multi-modal transformer to model local weather dynamics at the station level, taking advantage of both gridded numerical weather products and weather station observations.
4. We evaluate our models against a range of data-driven and non-data-driven off-grid weather forecasting methods. Amongst those, our transformer model achieves the best performance. It decreases the average error by 36% compared to the best performing ML baseline model, which in turn reduces the mean forecast error by 34% compared to the best performing non-ML baseline model (interpolated HRRR reanalysis).
5. We conduct an ablation of inputs and observed that all ML models improve significantly when NWP are used as inputs. For example, a transformer with HRRR input achieves 50% of the error of a transformer without HRRR, indicating that—even in the presence of historical station data—large-scale atmospheric dynamics inform local weather patterns.

2 Related Work

Dynamical Downscaling The mismatch between the large-scale weather/climate simulation and the local observations is a long-standing problem in atmospheric sciences. Downscaling techniques have been widely used to alleviate the mismatch by improving the resolution and debiasing of large-scale weather/climate simulations. One type of downscaling technique is dynamical downscaling, which uses high-resolution regional models

or limited-area models that are nested within global numerical models to generate finer-scale simulations. This approach explicitly solves physical equations governing atmospheric dynamics and thermodynamics at a higher resolution, allowing for a more detailed representation of local topography, land-atmosphere interactions, and mesoscale weather patterns. Prominent models used for dynamical downscaling include the Weather Research and Forecasting (WRF) model (Skamarock et al., 2008) and the Regional Climate Model (RegCM) (Giorgi et al., 2012). Despite its ability to provide physically consistent and high-fidelity representations of local dynamics, dynamical downscaling is computationally expensive, requiring significant resources for running high-resolution simulations over extended periods. Moreover, biases and uncertainties from the driving global model can propagate into the regional model, affecting accuracy.

Statistical Downscaling Statistical downscaling, on the other hand, leverages statistical or machine learning techniques to establish empirical relationships between large-scale coarse-resolution model outputs and local weather observations. Traditional statistical downscaling methods include linear regression models (Wilby, 1998), canonical correlation analysis (Storch et al., 1993), and analog method (Zorita & Storch, 1999). These methods are extensively evaluated and compared in Hernanz et al. (2022). More recently, deep learning-based approaches, such as convolutional neural networks (CNNs) (Vandal et al., 2017) and generative adversarial networks (GANs) (Stengel et al., 2020), have been explored for downscaling tasks. Compared to dynamical downscaling, statistical downscaling is computationally more efficient and can be easily adapted to different regions and variables. However, its performance depends on the availability of high-quality training data, and it may struggle with capturing physically consistent interactions beyond the training data.

Gridded Weather Forecasting Weather forecasting has long been a challenging problem in atmospheric sciences, with efforts dating back centuries. Since the advent of numerical weather prediction (NWP) in the mid-20th century, most forecast simulations have been conducted on a regular grid, dividing the atmosphere into evenly spaced discrete points to solve complex partial differential equations. This grid-based approach has remained the foundation of many numerical weather forecasting models such as the Integrated Forecast System (ECMWF, 2022) and High-Resolution Rapid Refresh (Dowell et al., 2022). In recent years, machine learning (ML) has gained traction as a promising tool in weather forecasting (Bauer et al., 2015), offering new techniques to improve accuracy and computational efficiency. These ML weather models can be roughly divided into two categories: end-to-end models and foundation models. FourCastNet (Pathak et al., 2022), GraphCast (Lam et al., 2023), Pangu-Weather (Bi et al., 2023), AIFS (Lang et al., 2024) and NeuralGCM (Kochkov et al., 2024) are end-to-end models trained directly to make weather forecasts. In contrast, AtmoRep (Lessig et al., 2023), ClimaX (Nguyen et al., 2023), Aurora (Bodnar et al., 2024) and Prithvi WxC (Schmude et al., 2024) are foundation models that are first trained with a self-supervision task and then fine-tuned for weather forecasting. However, the training data for ML models largely stem from traditional gridded numerical simulations such as ERA5 (Hersbach et al., 2020). As a result, the ML models themselves still typically maintain the grid-based paradigm even within their more modern forecasting approach. One major disadvantage of gridded weather forecasting is that it is usually limited by its fixed resolution such that it cannot accurately reflect fine-grained local weather patterns (although efforts towards limited area modeling have recently been made (Oskarsson et al., 2023)). Other works focusing on increasing the forecast resolution (Harder et al., 2023; Yang et al., 2023; Prasad et al., 2024) exist, but their methods are mostly tested on synthetic datasets. Work meant to correct ERA5 forecasts exists (Mouatadid et al., 2023), but focus on sub-seasonal forecast at coarse spatial resolution rather than local weather forecasting. In this work, we propose multi-modal deep learning models which can effectively downscale gridded weather forecasts to match real-world local weather dynamics.

Off-Grid Weather Forecasting Even though gridded weather forecasting is the main focus of the ML community, there have been several attempts to forecast weather off-grid. Bentsen et al. (2023) applied a GNN to forecast wind speed at 14 irregularly spaced off-shore weather stations, each of which was treated as a node within the graph. The model input is the historical trajectory of weather variables recorded at each station. This work has two limitations: the forecasting region is small, only covering 14 stations, and it only considers a single input modality of station historical measurements. MetNet-3 (Andrychowicz et al., 2023) takes another approach to off-grid weather forecasting. It trains a U-Net-like transformer (Ronneberger et al., 2015) model that takes multi-modal inputs including weather station observations, satellite imagery, and assimilation products to predict weather at stations. However, both input and output station data are re-gridded to a high resolution mesh ($4 \text{ km} \times 4 \text{ km}$), which distorts the off-grid data’s original granularity.

Graph Neural Network for Physical Simulation Graph neural networks (GNNs) are a type of deep learning model designed to operate on data structured as graphs, where entities are represented as nodes and their relationships as edges. GNNs provide flexibility to process data with non-Euclidean structures. A GNN learns to capture relationships between nodes by iteratively passing and aggregating information between neighboring nodes, and updating node representations based on their connections. Recently, GNNs have been widely used in physical system simulation. For example, the 2D Burgers’ equation can be effectively solved on both a regular and an irregular mesh with GNNs such as MAgNet (Boussif et al., 2022) and MPNN (Brandstetter et al., 2023). Sanchez-Gonzalez et al. (2020) used a GNN to simulate particle dynamics in a wide variety of physical domains, involving fluids, rigid solids, and deformable materials interacting with one another. GraphCast (Lam et al., 2023) even showed that a 3D GNN is capable of simulating a global gridded atmospheric system. These successful use cases of GNNs motivate us to apply a graph network to our task for localized off-grid weather forecasting.

Transformer as Building Blocks for Weather Models Transformers (Vaswani et al., 2023; Dosovitskiy et al., 2021) have become the fundamental components of modern weather foundation models due to their ability to learn complex spatial-temporal relationships from large-scale atmospheric data. These models, such as AtmoRep (Lessig et al., 2023) and ClimaX (Nguyen et al., 2023), leverage transformers to pretrain on diverse meteorological datasets, enabling them to generalize across various forecasting tasks. One key advantage of transformers is their flexibility in handling irregularly spaced data, making them well-suited for off-grid applications. Specifically, transformers treat irregularly spaced data as a sequence of tokens, and use self-attention mechanisms to process them without relying on a grid-based structure. Transformers provide a powerful and flexible solution for off-grid weather forecasting.

3 Methods

In this work, we investigate two deep learning models for localized weather forecasting: a message passing neural network (MPNN, Gilmer et al. (2017); Pfaff et al. (2021)) and a transformer (Vaswani et al., 2023; Dosovitskiy et al., 2021). Both models ingest multi-modal Earth observation data and are trained to forecast weather at the station level with the aid of large-scale weather predictions. At its core, these two models use past local weather station observations to forecast the weather variables of interest at different lead times into the future. This structure is then extended with the gridded output of a large-scale weather model (could be NWP or ML) known to provide accurate forecasts on a broad scale, but lacking accuracy at fine scales (e.g., large-scale models largely neglect surface friction when modeling wind fields, see Figures 1 and 2). By integrating large-scale forecasts with localized weather data, we can view the task as a correction of large-scale forecasts rather than forecasting *de novo*; that is, our model aims to correct the large-scale forecast toward the local reality based on prior local observa-

tions. This setup enables our model to achieve accurate off-grid near-surface weather forecasting.

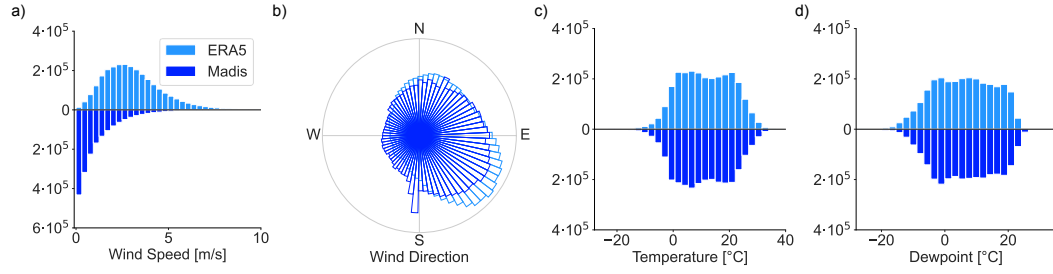


Figure 2. Comparison of data collected by weather stations (MADIS) and linearly interpolated global reanalysis data (ERA5). For both ERA5 and MADIS data, (a) histogram of wind speed, (b) radial histogram of wind direction, (c) histogram of temperature and (d) histogram of dewpoint for the study region from January to December 2023. Large differences, especially in wind speed, are apparent between local wind observations and global wind products. ERA5, which is the target that most ML weather models emulate, does not capture local wind dynamics.

3.1 Model

The fundamental idea of weather forecasting is to predict the weather at a future time $l\Delta t$ (the lead time), given a set of information:

$$\mathbf{w}(t + l\Delta t) = F(\dots), \quad (1)$$

where t is the current time, \mathbf{w} is a vector of weather observations at n different weather stations ($\mathbf{w} = [w_0, \dots, w_n]$), and F is the function mapping input variables to the forecast. When using local historical data to predict the weather, the function F takes the form:

$$\mathbf{w}(t + l\Delta t) = F(\mathbf{w}(t - b\Delta t : t)), \quad (2)$$

where $b\Delta t$ is the number of past time steps considered, called back hours. This equation thus maps past weather data to future weather data, only considering the local weather stations (Figure 3a).

We propose to change the nature of the problem, transforming the arguably hard task of forecasting to correcting an existing weather forecast. We thus introduce an external global weather forecast \mathbf{g} , and modify the function F :

$$\mathbf{w}(t + l\Delta t) = F(\mathbf{w}(t - b\Delta t : t), \mathbf{g}(t - b\Delta t : t + l\Delta t)). \quad (3)$$

The global weather forecast covers the period from the back hours all the way to the lead time (Figure 3b). The function F can take the form of any model, for instance a transformer or a GNN, which considers spatial correlation, i.e. the connections between the weather stations, in addition to temporal correlation.

3.1.1 Transformer

We implement a transformer model for the prediction function F . The transformer model is an encoder-only architecture similar to vision transformers (Dosovitskiy et al.,

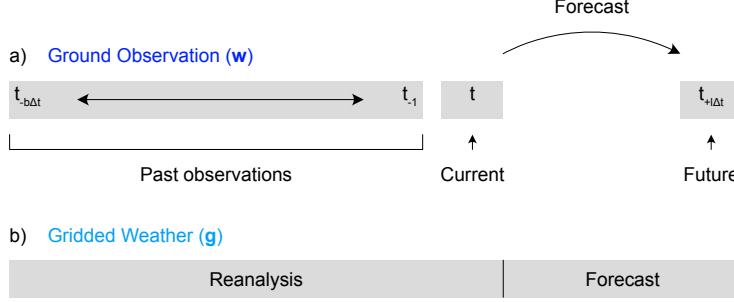


Figure 3. Schematic of the forecasting task. (a) The ground stations’ past observations $\mathbf{w}(t - b\Delta t : t)$ are used to forecast the weather conditions at a given lead time $\mathbf{w}(t + l\Delta t)$. (b) By introducing a gridded weather model’s past and future data \mathbf{g} , the setup is transformed from a pure forecasting problem to a correction problem, where the future gridded weather data are corrected towards local observations.

2021). It treats weather measurements at each station as a token, then applies a series of self-attention layers to the tokens to learn spatial dependencies. Given the relative small size of the study area (Northeastern US), the transformer ingests all available weather stations at once. To integrate the gridded large-scale weather data, each station token is concatenated with the large-scale weather data at the grid cell closest to the station.

The overall structure of the transformer is given in Figure 4. Ground observation data w at each station are combined with its nearest neighbor gridded weather data g for N stations, and passed through an MLP embedder to create token embeddings. These token embeddings are then paired with positional embeddings and passed through a transformer encoder. Finally, an MLP prediction head is applied to generate weather forecasts for each of the N stations.

Since the transformer encoder is the main component of the transformer model, we provide more details. For a complete description of the transformer encoder, please refer to the original paper (Dosovitskiy et al., 2021). The encoder consists of a series of encoding blocks, each containing a multi-head self-attention mechanism and a feed-forward network. The multi-head self-attention mechanism allows the model to attend among input station tokens to learn representations that consider station-to-station spatial dependencies. The feed-forward network is a simple two-layer MLP aiming to refine the learned representations.

Multi-Head Self-Attention Each head of the multi-head self-attention mechanism computes a new representation for each input token using query (\mathbf{Q}), key (\mathbf{K}), and value (\mathbf{V}) matrices. These matrices are computed from the input tokens using learned linear projections, that is, $\mathbf{Q} = \mathbf{X}\mathbf{W}_{\mathbf{Q}}$, $\mathbf{K} = \mathbf{X}\mathbf{W}_{\mathbf{K}}$, and $\mathbf{V} = \mathbf{X}\mathbf{W}_{\mathbf{V}}$. $\mathbf{W}_{\mathbf{Q}}, \mathbf{W}_{\mathbf{K}}, \mathbf{W}_{\mathbf{V}}$ are the learned matrices transforming token matrix $\mathbf{X} \in \mathbb{R}^{N \times d}$ to $\mathbf{Q}, \mathbf{K}, \mathbf{V} \in \mathbb{R}^{N \times d}$. The new representation for each input token is then produced by computing a weighted sum of the input token values:

$$\text{Attention}(\mathbf{Q}, \mathbf{K}, \mathbf{V}) = \text{softmax}\left(\frac{\mathbf{Q}\mathbf{K}^T}{\sqrt{d}}\right)\mathbf{V}. \quad (4)$$

In multi-head self-attention, this process is repeated h times with different learned projections, and the results are concatenated and linearly transformed to produce the final output:

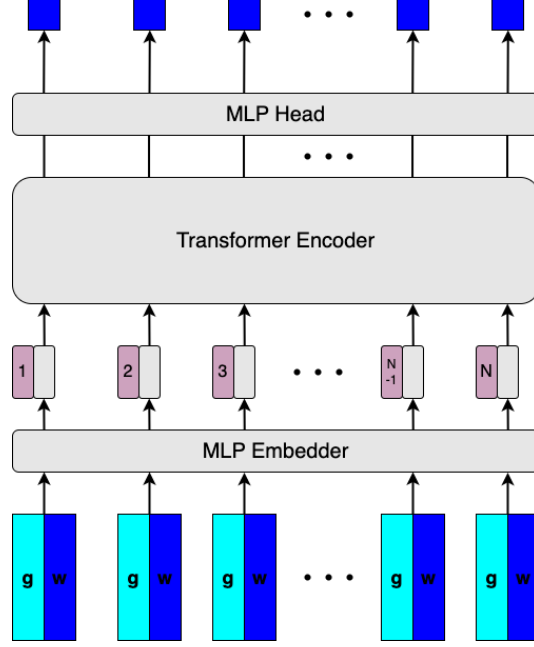


Figure 4. Transformer model for off-grid weather forecasting. Gridded weather \mathbf{g} and ground observation \mathbf{w} at N stations are combined using an MLP embedder to create token embeddings. These token embeddings are then concatenated with positional embeddings and passed through a transformer encoder, followed by an MLP prediction head, to generate forecasts for each station.

$$\text{MultiHead}(\mathbf{X}) = \text{Concat}(\text{head}_1, \dots, \text{head}_h) \mathbf{W}_{\mathbf{O}}, \quad (5)$$

where $\text{head}_i = \text{Attention}(\mathbf{X} \mathbf{W}_{\mathbf{Q}}^i, \mathbf{X} \mathbf{W}_{\mathbf{K}}^i, \mathbf{X} \mathbf{W}_{\mathbf{V}}^i)$ and $\mathbf{W}_{\mathbf{O}} \in \mathbb{R}^{hd \times d}$ is the output projection matrix.

Feed-Forward Network and Residual Connections

Following the multi-head self-attention mechanism, each encoder block includes a feed-forward network (FFN) that is independently applied to each token. This component consists of two linear transformations with a non-linear activation in between, typically using the Rectified Linear Unit (ReLU) or GELU activation. Formally, given an input token representation $\mathbf{x} \in \mathbb{R}^d$, the FFN is defined as:

$$\text{FFN}(\mathbf{x}) = \max(0, \mathbf{x} \mathbf{W}_1 + \mathbf{b}_1) \mathbf{W}_2 + \mathbf{b}_2, \quad (6)$$

where $\mathbf{W}_1 \in \mathbb{R}^{d \times d_h}$ and $\mathbf{W}_2 \in \mathbb{R}^{d_h \times d}$ are learned weights, and d_h is the hidden dimension which is typically larger than d (e.g., $d_h = 4d$). $\mathbf{b}_1 \in \mathbb{R}^{d_h}$ and $\mathbf{b}_2 \in \mathbb{R}^d$ are the biases within the FFN. To facilitate optimization and preserve gradient flow, each sub-layer (i.e., the self-attention and the FFN) is wrapped with a residual connection followed by layer normalization (Ba et al., 2016).

3.1.2 Message Passing Neural Network (MPNN)

As a baseline, we also implement the prediction function F as a GNN. Each weather station naturally becomes a node of a graph. The weather station graph is constructed

with Delaunay triangulation (Delaunay, 1934) on the geographic coordinates of the stations. Delaunay triangulation links each station to a few nearby neighbors, giving balanced connections in all directions while maintaining sparsity and efficient message-passing.

To integrate the large-scale weather data (past and future), the weather station graph is extended to include NWP grid cell nodes (Figure 5). In this heterogeneous graph, each weather station node is connected to the o closest large-scale weather data grid cell nodes (4 in the example in Figure 5, but 8 in the experiments later). These edges are uni-directional, meaning the information flows from global to local, but not back. The heterogeneous graph constructed for our study area is given in Figure A1.

MPNNs are a type of GNNs that operate on a given graph structure by passing messages between connected nodes. The messages consist of information contained in the nodes as well as in the edges connecting the nodes. The nodes are updated with the incoming messages. This architecture can be trained for different tasks, such as predicting at a node level (e.g., simulating particle dynamics) and at a graph level (e.g., classifying chemicals). We follow the implementation of MPNN as described in Brandstetter et al. (2023). It works in three steps: encode, process, and decode (Battaglia et al., 2018; Sanchez-Gonzalez et al., 2020).

Encode This step encodes the information contained in each node and transforms it into a latent feature. Station nodes and large-scale weather data grid cell nodes are encoded separately.

$$f_i \leftarrow \alpha(w_i(t - b\Delta t : t), p_i), \quad (7)$$

$$h_r \leftarrow \psi(g_r(t - b\Delta t : t + l\Delta t), p_r), \quad (8)$$

where w_i is a vector containing the observed weather variables at station node i ; g_r is the large-scale weather data at grid cell node r ; p the coordinates; and α, ψ are encoding neural networks, here a simple two-layer MLP. The f, h denote embedded features at each node; they extract the essential information contained in station nodes and grid cell nodes separately.

Process This step processes each node’s feature with incoming messages that aggregate information from its connected neighbors. As we are interested in the weather at the station level, only the station node features are updated. Since each station node has two types of neighbors, (1) other station nodes and (2) large-scale weather data grid cell nodes, the update procedure has two forms as well. First, update station i with its station neighbors j :

$$\mu_{ij} \leftarrow \beta(f_i, f_j, w_i(t - b\Delta t : t) - w_j(t - b\Delta t : t), p_i - p_j), \quad (9)$$

$$f_i \leftarrow f_i + \gamma \left(f_i, \frac{1}{|\mathcal{N}(i)|} \sum_{j \in \mathcal{N}(i)} \mu_{ij} \right) \quad (10)$$

μ_{ij} is the produced message passing from station node j to station node i . Station node feature f_i is then updated according to eq. 10 with the message from its station neighbors whose indices are in $\mathcal{N}(i)$. β and γ are two-layer MLPs completing the process.

Second, update with the large-scale weather data grid cell node neighbors:

$$\nu_{ir} \leftarrow \chi(h_r, f_i, p_i - p_r) \quad (11)$$

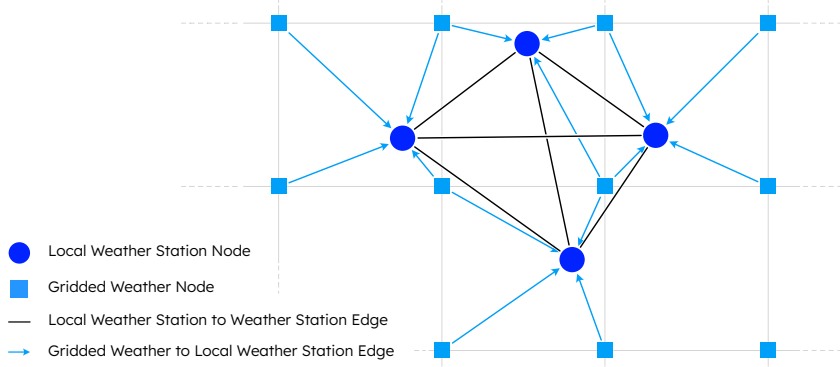


Figure 5. Simplified diagram of our multi-modal graph. Local weather stations form the base graph, with each station node connected to its neighbors using Delaunay triangulation. The gridded numerical weather dataset is arranged on a regular mesh, with each station node connected to its o closest gridded nodes (4 in this example). Station nodes pass messages to each other in bi-directional edges; grid nodes pass messages to station nodes, but not vice-versa.

$$f_i \leftarrow f_i + \omega \left(f_i, h_r, \frac{1}{|\mathcal{M}(i)|} \sum_{r \in \mathcal{M}(i)} \nu_{ir} \right), \quad (12)$$

Similarly, ν_{ir} is the message passing information at weather data grid cell node r to station node i . Station node feature f_i is updated with message ν_{ir} by eq. 12, where $\mathcal{M}(i)$ contains all cell nodes connected to station node i . χ and ω are two-layer MLPs containing all trainable parameters within the process.

Decode The decoding step then maps the final station node feature to the weather variables at the given lead time:

$$w_i(t + l\Delta t) = \phi(f_i), \quad (13)$$

with ϕ a two-layer MLP.

Predictive Graph Model Putting everything together, weather variables at all stations are predicted by:

$$\mathbf{w}(t + l\Delta t) = \mathbf{D} \circ \hat{\mathbf{P}}_2 \circ \dots \circ \mathbf{P}_k \circ \dots \circ \hat{\mathbf{P}}_1 \circ \mathbf{E}(G). \quad (14)$$

The multi-modal input data is organized as a graph G . Its nodes are first encoded by \mathbf{E} . Station nodes are then updated with information from grid cell nodes by $\hat{\mathbf{P}}_1$. After the grid node message passing, the station nodes are updated internally by multiple layers of station node message passing \mathbf{P}_k . Following that, the station nodes ingest grid cell node information one more time by $\hat{\mathbf{P}}_2$. Finally, the station nodes are decoded by \mathbf{D} to produce the weather variables of interest.

3.2 Data

Our goal in this work is to forecast the weather at precise locations, integrating historical observations, and supplemented with global gridded weather products. To do this, we prepare following datasets: (1) point-based weather observations from MADIS sta-

tions, (2) gridded reanalysis data from ERA5, and (3) gridded weather forecast products from HRRR. The details of our curated multi-modal dataset are summarized in Table A1. ERA5 has lower resolution and is less optimized for US weather modeling than HRRR, but is widely used as a target for foundation models and is thus a good candidate for a “perfect” forecast. Additionally, performing experiments with both allows us to study how the quality of the global weather data affects weather forecasting at station level.

MADIS The Meteorological Assimilation Data Ingest System (MADIS¹) is a database provided by the National Oceanic and Atmospheric Administration (NOAA) that contains meteorological observations from stations covering the entire globe. MADIS ingests data from NOAA and non-NOAA sources, including observation networks from US federal, state, and transportation agencies, universities, volunteer networks, and data from private sectors like airlines as well as public-private partnerships like the Citizen Weather Observer Program. MADIS provides a wide range of weather variables from which we curated 10m wind speed, 10m wind direction, 2m temperature, and 2m dewpoint temperature for this study. In this work, we focus on stations over the Northeastern US region (Maine, New Hampshire, Vermont, Massachusetts, Rhode Island, Connecticut, New York, New Jersey, and Pennsylvania, see Figure 1a). We only keep averaged hourly observations with the quality flag “Screened” or “Verified”. Additionally, only stations with at least 90% of data of sufficient quality are considered. Across the study region, this leaves us with 358 stations (Figure 1a, dark blue arrows). We processed 5 years of data from 2019 to 2023.

ERA5 The ECMWF Reanalysis v5 (ERA5) climate and weather dataset (Hersbach et al., 2020) is a gridded reanalysis product from the European Center for Medium-Range Weather Forecasts (ECMWF) that combines model data with worldwide observations. The observations are used as boundary conditions for numerical models that then predict various atmospheric variables. ERA5 is available as global hourly data with a $0.25^\circ \times 0.25^\circ$ resolution, which is 31 km/pixel at the equator, spanning 1950–2024. It includes weather both at the surface and at various pressure levels. We curated 5 years (from 2019 to 2023) of surface variables: 10m wind u , 10m wind v , 2m temperature, and 2m dewpoint temperature.

HRRR The High-Resolution Rapid Refresh (HRRR, Dowell et al. (2022)) model, developed by NOAA, is a numerical weather prediction system that provides high-resolution, short-term weather forecasts for the continental US and Alaska. Designed for detailed and timely predictions, HRRR operates with a grid spacing of approximately 3 kilometers and updates hourly, incorporating real-time radar, satellite, and observational data. Each update generates forecasts up to 18 hours ahead, along with a reanalysis of the current atmospheric state (considered ground truth). For this study, we curated 5 years (2019–2023) of surface variables from HRRR, including 10-meter wind components (u and v), 2-meter temperature, and 2-meter dewpoint temperature.

3.3 Experiments

Forecast Setup In this work, models are trained to predict 10m wind vector (u and v), 2m temperature, and 2m dewpoint temperature all together at each MADIS station. To predict these variables at each weather station, we first provide the model with prior measurements of 10m wind u , 10m wind v , 2m temperature, and 2m dewpoint temperature at each MADIS node. Similarly, at each grid cell of ERA5 or HRRR, the inputs are 10m u , 10m v , 2m temperature, and 2m dewpoint temperature (from past and future). For all inputs, the temporal resolution is 1 hour. The transformer model is given all weather stations as a sequence of tokens, and each station token is concatenated with

¹ <https://madis.ncep.noaa.gov/>

the nearest NWP grid cell. In the MPNN graph, each MADIS node is connected to its MADIS neighbors based on the Delaunay triangulation. Then each MADIS node is also connected to its 8 nearest NWP grid cells based on the Euclidean distance (Figure A1).

All models are tasked with predicting 10m u , 10m v , 2m temperature, and 2m dewpoint temperature at each MADIS node for different lead times: 1, 2, 4, 8, 16, 24, 36 and 48 hours, for which we train one model each. The model is trained with data from 2019 to 2021, validated on 2022, and tested on 2023. There are $\sim 8,760$ time steps per year for each of the 358 stations. In total, we obtain a training set of $\sim 26,280$ samples, a validation set of $\sim 8,760$ samples, and a test set of $\sim 8,760$ samples. The model uses 48 hours of MADIS back hours (Figure 3a), i.e. the weather observations from the previous 48 hours, including the current observation, to predict forward. When including large-scale gridded weather data, the model is given the time steps from the back hours to the lead time (Figure 3b), providing a full temporal view of large scale dynamics. Since the HRRR forecast is limited to 18 hours ahead, models use HRRR forecast data up to 18 hours for lead times beyond this range.

Baseline Methods Besides the MPNN model, we also compare the transformer against a series of other baseline forecasting methods: interpolated ERA5, interpolated HRRR, MADIS persistence, and an MLP. Interpolated ERA5 or HRRR refers to a nearest neighbor interpolation of ERA5 or HRRR grid cells to a MADIS station location, meaning each station location takes ERA5 or HRRR value at the grid cell closest to the station. The MADIS persistence simply shifts the observation by the lead time and will perform well if the temporal auto-correlation of weather variables is high. The MLP provides a baseline model with an architecture mirroring the architecture of the MPNN, but with no station-to-station message passing spatial structure. For the MLP experiments, the gridded weather data is interpolated at the weather stations and used as an additional input. The same MLP is tasked with forecasting at all stations; we also tried training a separate MLP for each station but did not observe better performance.

Study of Gridded Weather Product Contributions The MLP, MPNN, and transformer are run with and without gridded weather data to assess how much performance gain for localized weather forecasting comes from knowing large-scale weather dynamics. When including gridded weather data, models are run with ERA5 reanalysis, HRRR forecast or with HRRR reanalysis. Both HRRR forecast and reanalysis are used to assess how the error in large-scale weather forecasts are propagated to the localized weather forecasting. In addition, ERA5 has lower resolution than HRRR; HRRR is optimized for the US while ERA5 is optimized for the globe. To see how this data quality difference affects weather forecasting at the station level, models run with ERA5 reanalysis are also compared to those run with HRRR reanalysis.

4 Results

We report the model performance on the 2023 test set for 10m wind, 2m temperature, and 2m dewpoint separately. The metric used for 2m temperature and dewpoint is the standard root mean square error (RMSE). As for 10m wind (a vector containing u and v components), the metric used is the mean magnitude of the wind vector error ($\sqrt{\Delta u^2 + \Delta v^2}$). Figure 6 summarizes forecast performance of different models at various lead times with respect to all three variables. Detailed numerical results are provided in Table A2, Table A3, and Table A4.

Transformer is the best forecasting model for all variables The second column of Figure 6 shows that the transformer model outperforms the GNN and MLP models for all variables whether gridded HRRR reanalysis data is used or not. When gridded HRRR reanalysis data is used, the transformer model also performs better than the non-ML models such as the persistence model and the gridded weather interpolation mod-

els for all variables as demonstrated in the first column of Figure 6. Specifically, for 10m wind, the transformer model with HRRR-R (HRRR reanalysis data) achieves a lead-hour averaged wind vector error of 0.48 m/s, which is 22% lower than the next best performing ML model, the MLP model with HRRR-R. It is also 49% lower than the persistence model and 80% lower than the HRRR-R interpolation models. In terms of 2m temperature, the transformer model with HRRR-R reduces the lead-hour averaged RMSE by 41% compared to the MLP model with HRRR-R. Its RMSE is also 73% lower than the

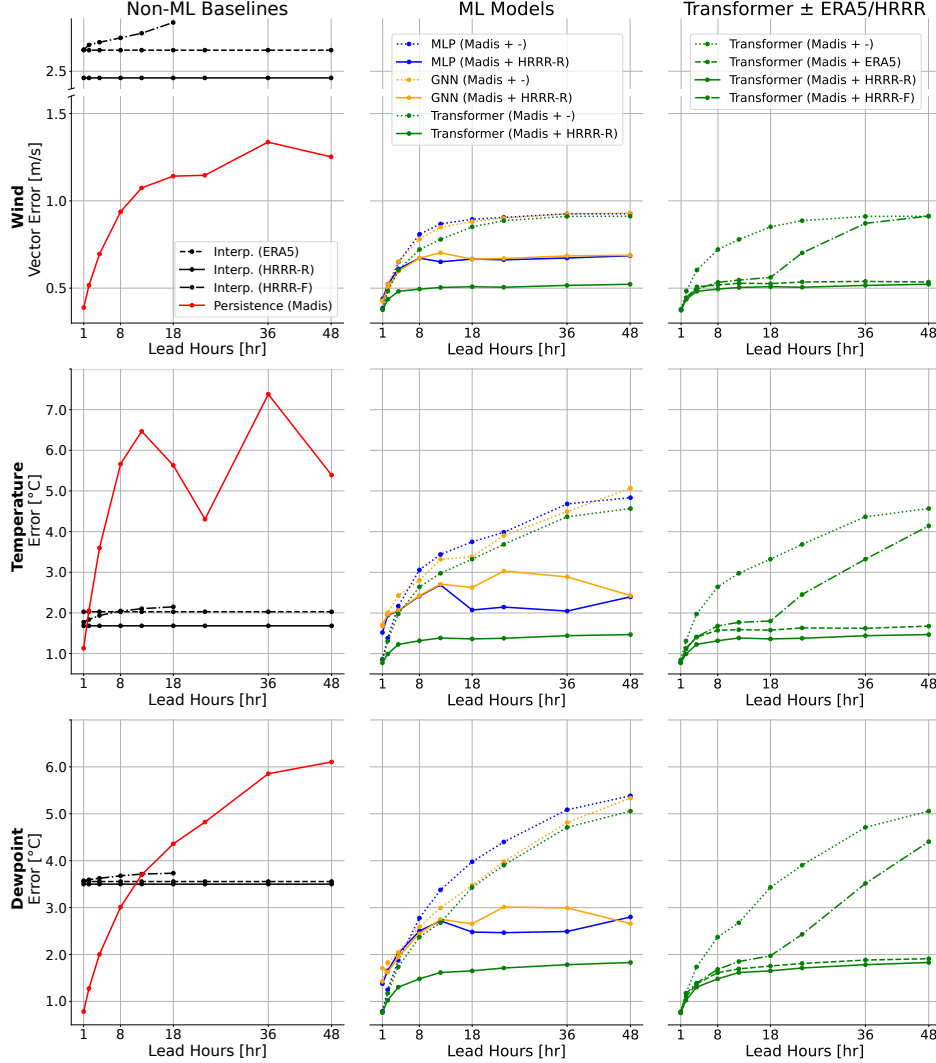


Figure 6. Model forecast errors with respect to 10m wind, 2m temperature, and 2m dewpoint at various lead times. From top to bottom: model performance on 10m wind, 2m temperature, and 2m dewpoint is shown as a function of lead time. The left column shows naive non-ML model performance, the middle column shows ML model performance with/without gridded weather data, and the right column shows model performance of only transformer models but with different types of gridded weather data as inputs.

persistence model and 25% lower than the HRRR-R interpolation model. In addition, the transformer model with HRRR-R achieves a lead-hour averaged 2m dewpoint RMSE of 1.46 Celsius degrees, which is 36% lower than the MLP model with HRRR-R, 59%

lower than the persistence model, and 58% lower than the HRRR-R interpolation model.

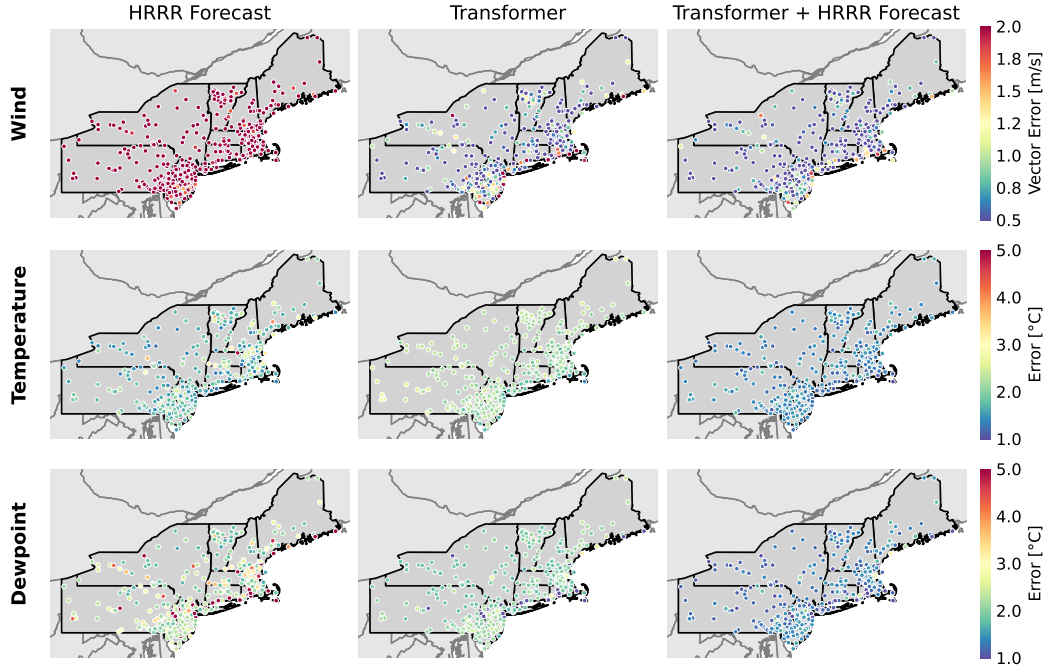


Figure 7. Forecast errors of the different methods shown for each MADIS station, averaged over the lead times less than 18 hours. From top to bottom: forecast error spatial distribution is presented for 10m wind, 2m temperature, and 2m dewpoint. The transformer models with HRRR forecast (third column) show significantly lower errors than the naive interpolations of HRRR forecast (first column).

Gridded weather data is beneficial for all ML models The second column of Figure 6 shows that all ML models perform better when gridded HRRR reanalysis data is used. This performance boost is also true across all variables. For example, the HRRR-R data helps the transformer model reduce lead-hour averaged wind vector error by 33%, temperature RMSE by 56%, and dewpoint RMSE by 49%, compared to the counterparts without HRRR-R.

The quality of gridded weather data is critical for ML models The quality of gridded weather data is directly reflected in the performance of resultant ML models who use it. As shown in the first column of Figure 6, HRRR-R interpolation outperforms HRRR-F (HRRR forecast) interpolation; and ERA5 interpolation achieves performance in between the two. As a result, transformer models with gridded weather data share the same order of performance: with HRRR-R better than with ERA5, and with ERA5 better than with HRRR-F (the third column of Figure 6). Still, all transformer models with gridded weather data outperform the one without, as gridded data provides a future outlook of larger scale weather patterns. Additionally, there is a noticeable increase in errors for transformer models with HRRR-F beyond the 18 hour lead time, which aligns with the fact that HRRR only provides forecast data up to 18 hours ahead.

Wind prediction benefits the most from combining gridded weather data with station data The transformer model combining HRRR-R and station measurements reduces wind vector error by 80%, temperature RMSE by 25%, and dewpoint RMSE by 58%, compared to naive HRRR-R interpolation. The wind vector error is the most

reduced, followed by dewpoint RMSE, and temperature RMSE is the least reduced. We speculate that local wind is the variable that is the most sensitive to local environment and/or modeled the most poorly by global gridded models, followed by dewpoint and temperature. This is also observed in Figures 1 and 2: temperature and dewpoint ERA5 reanalysis data correlate well with the station data, while wind has much lower correlation.

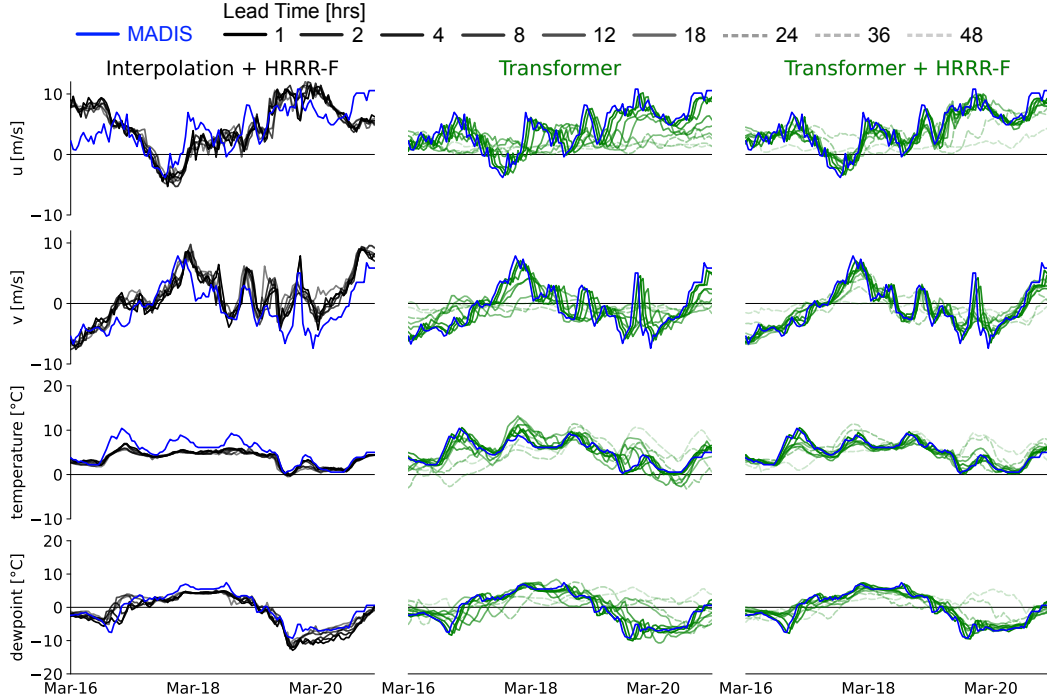


Figure 8. Example time series illustrating the transformer model’s integration of HRRR-F into its prediction. From top to bottom: time series of 10m u and v components, 2m temperature, and 2m dewpoint are presented. Each panel has the MADIS ground truth in blue, and the predictions at increasing lead times displayed with decreasing saturation. This station happens to be the one where the transformer + HRRR-F model performs the worst on average. For this station and time snippet the interpolated HRRR-F appears relatively accurate, and the transformer is able to integrate the HRRR-F data well.

Transformer model with HRRR forecast improves local weather predictions across all stations Figure 7 shows that how transformer models’ prediction errors are distributed across all stations. Compared to the naive interpolations of HRRR forecast (first column), the transformer model informed by only station measurements (second column) show lower errors for 10m wind and 2m dewpoint, but slightly higher errors for 2m temperature. This indicates that wind and dewpoint are more sensitive to local environments; while temperature is more dominated by large scale atmospheric conditions. When using HRRR-F (third column), the transformer model’s performance is further improved, especially for 2m temperature and 2m dewpoint. The resultant transformer model shows significantly lower errors than the naive interpolations of HRRR-F for all three variables. This error reduction is seen across all stations, indicating that the transformer model is able to generalize well across different locations. Interestingly, the transformer model shows relatively large wind errors at stations along the coastline. It may be due to the fact that these stations are situated in an open environment, thus

experiencing similar conditions represented by gridded weather models. As a results, they benefit less from local measurements.

Transformer model integrates HRRR forecast data well Figure 8 shows, for different models, a snippet of time series of forecasted 10m wind u and v components, 2m temperature, and 2m dewpoint at the station with the worst forecast performance for the transformer model with HRRR-F. Unlike at many other stations, naive HRRR-F interpolation for this location agrees with the local MADIS data well, especially for 10m wind components and 2m temperature (c.f. Figure A4 for a time series where the naive interpolation doesn’t follow the MADIS observation as well). This allows us to evaluate the transformer model’s ability to integrate HRRR forecast data. The transformer model integrates the HRRR forecast data well, consistently correcting it towards the local measurements, and ignoring it when needed (c.f. wind in Figure A4). The further out the lead time, the more it relies on the HRRR-F data, but still performs better than the interpolated HRRR-F. Meanwhile, without HRRR-F, the tranformer model fails for longer lead times; for instance, it trends toward predicting a flat wind vector, preferring to minimize error by predicting the average.

5 Discussion

Weather station observations and gridded weather data are complementary for successful local weather forecasting Discrepancies arise between weather station observations and gridded weather data, such as ERA5 and HRRR, due to the latter’s limitations in modeling terrain and land cover. We have shown that these local surface characteristics significantly influence local weather patterns, particularly wind (Figure 1). Meanwhile, the high forecast error associated with MADIS persistence shows that current local weather conditions do not reliably indicate future conditions. Accurate fine-grained weather forecasting therefore requires a model that accounts for both local conditions and the inherent variability of local weather patterns across time. Gridded weather products and historical station data provide key complementary information for capturing local weather dynamics. By combining these two datasets, we achieve a local weather forecasting model that is significantly more accurate than ERA5 or HRRR (and, by extension, current gridded ML weather models). The need for weather station data to capture local conditions is especially evident where stations situated amidst buildings or trees experience conditions that differ significantly from those represented by gridded weather models (Figure A5). This is most apparent inland, where the reduction in error of the gridded dataset is greatest, but also on the coast for more sheltered weather stations.

The dynamic spatial attention mechanism gives the transformer an edge in local weather forecasting In this work, we explore three ML models: a transformer, a GNN, and an MLP, that can integrate both local weather station observations and gridded weather data successfully for local weather forecasting. When predicting local weather using only local data, all ML models achieve respectable performances. With the introduction of ERA5 or HRRR, all models successfully incorporate large-scale atmospheric dynamics from ERA5 or HRRR, thereby improving predictions at longer lead times. Among the three models, the transformer model shows the best performance. This is likely due to the transformer’s dynamic spatial attention mechanism. It enables the transformer to attend to the relevant stations according to current weather conditions. In contrast, the GNN can only attend to predefined station locations, and the MLP is unable to attend to any other stations besides each station itself.

Direct input of station data helps make predictions at station locations more accurate Using both station data and gridded weather data for local weather forecasting is not new. For example, Vaughan et al. (2024) trained an end-to-end ML local weather forecasting model that first assimilates station data into gridded weather data;

then makes time stepping into the future in the gridded space; lastly, downscales the gridded weather forecast to the station locations. However, their model’s performance is not as good as the transformer model in this work, especially for surface wind predictions, where their wind prediction error caps out at 1 m/s, while the transformer model in this work gets it down to 0.5 m/s. This significant performance gap may be attributed to the fact that when making final predictions at station locations, their model only uses the gridded weather forecast as input but ignores the station data used to assimilate the gridded fields. In other words, their model lacks the direct input of station data when making station-level predictions. In contrast, the transformer model in this work directly uses the station data as input and combines with gridded data when making predictions. It gives the transformer model a better understanding of the station location weather patterns, which is crucial for local weather forecasting. In summary, our approach provides a phase shift in local weather forecasting accuracy when directly combining station data with gridded weather data. All the ML based gridded weather forecasting models, whether foundation models or end-to-end models, will be limited in local weather forecasting accuracy without the direct input of station data.

6 Conclusion

This work demonstrates the use of a multi-modal transformer for downscaling gridded weather forecasts and improving the accuracy of off-grid predictions. Our model addresses the inherent bias in gridded numerical weather products like ERA5 and HRRR. By concatenating both MADIS weather station data and HRRR or ERA5 gridded weather data as input tokens, our transformer predicts off-grid weather conditions by leveraging both large-scale atmospheric dynamics and local weather patterns. In our evaluation of surface variable (10m wind, 2m temperature, and 2m dewpoint) prediction tasks, the transformer outperforms all baseline models. For instance, it achieved a 58% reduction in overall prediction error compared to HRRR reanalysis interpolation and a 36% improvement over the best-performing ML model. An ablation study, where numerical weather inputs were removed, all ML models performed significantly worse, highlighting the importance of incorporating large-scale atmospheric dynamics for accurate local predictions. This finding motivates the exploration of additional modalities, such as radar measurements and satellite imagery, which could further enhance local forecast accuracy. This research has significant implications for improving weather forecasting, particularly in high-value regions where weather stations can be installed. More accurate off-grid predictions can enhance weather-dependent decision-making in various sectors, including agriculture, wild-fire management, transportation, and renewable energy. Future work will focus on expanding the study area and exploring the integration of our transformer model with weather foundation models.

Code and Data Availability

The code and data for this paper can both be found on GitHub: <https://github.com/Earth-Intelligence-Lab/LocalizedWeatherGNN/>

Acknowledgments

We would like to thank and acknowledge Shell Information Technology International Inc. for funding the project, Peetak Mitra for helping processing the MADIS data, and our partners at Amazon Web Services and its Solutions Architects, Brian McCarthy and Dr. Jianjun Xu, for providing cloud computing and AWS technical support.

References

Andrychowicz, M., Espeholt, L., Li, D., Merchant, S., Merose, A., Zyda, F., . . .

- Kalchbrenner, N. (2023, July). *Deep Learning for Day Forecasts from Sparse Observations*. arXiv. Retrieved 2023-11-02, from <http://arxiv.org/abs/2306.06079> (arXiv:2306.06079 [physics]) doi: 10.48550/arXiv.2306.06079
- Ba, J. L., Kiros, J. R., & Hinton, G. E. (2016, July). *Layer Normalization*. arXiv. Retrieved 2025-04-15, from <http://arxiv.org/abs/1607.06450> (arXiv:1607.06450 [stat]) doi: 10.48550/arXiv.1607.06450
- Battaglia, P. W., Hamrick, J. B., Bapst, V., Sanchez-Gonzalez, A., Zambaldi, V., Malinowski, M., ... Pascanu, R. (2018, October). *Relational inductive biases, deep learning, and graph networks*. arXiv. Retrieved 2024-04-17, from <http://arxiv.org/abs/1806.01261> (arXiv:1806.01261 [cs, stat])
- Bauer, P., Thorpe, A., & Brunet, G. (2015, September). The quiet revolution of numerical weather prediction. *Nature*, 525(7567), 47–55. Retrieved 2024-09-30, from <https://www.nature.com/articles/nature14956> doi: 10.1038/nature14956
- Bentsen, L. \., Warakagoda, N. D., Stenbro, R., & Engelstad, P. (2023, March). Spatio-temporal wind speed forecasting using graph networks and novel Transformer architectures. *Applied Energy*, 333, 120565. Retrieved 2024-09-24, from <https://www.sciencedirect.com/science/article/pii/S0306261922018220> doi: 10.1016/j.apenergy.2022.120565
- Bi, K., Xie, L., Zhang, H., Chen, X., Gu, X., & Tian, Q. (2023, July). Accurate medium-range global weather forecasting with 3D neural networks. *Nature*, 619(7970), 533–538. Retrieved 2024-09-24, from <https://www.nature.com/articles/s41586-023-06185-3> (Publisher: Nature Publishing Group) doi: 10.1038/s41586-023-06185-3
- Bodnar, C., Bruinsma, W. P., Lucic, A., Stanley, M., Brandstetter, J., Garvan, P., ... Perdikaris, P. (2024). *Aurora: A Foundation Model of the Atmosphere*.
- Boussif, O., Assouline, D., Benabbou, L., & Bengio, Y. (2022, October). *MAGNet: Mesh Agnostic Neural PDE Solver*. arXiv. Retrieved 2023-11-28, from <http://arxiv.org/abs/2210.05495> (arXiv:2210.05495 [physics])
- Brandstetter, J., Worrall, D., & Welling, M. (2023, March). *Message Passing Neural PDE Solvers*. arXiv. Retrieved 2024-05-07, from <http://arxiv.org/abs/2202.03376> (arXiv:2202.03376 [cs, math])
- Delaunay, B. N. (1934). Sur la sphère vide. A la mémoire de Georges Voronoï. *Известия Российской академии наук. Серия математическая*, 6, 793–800.
- Dosovitskiy, A., Beyer, L., Kolesnikov, A., Weissenborn, D., Zhai, X., Unterthiner, T., ... Houlsby, N. (2021, June). *An Image is Worth 16x16 Words: Transformers for Image Recognition at Scale*. arXiv. Retrieved 2023-11-03, from <http://arxiv.org/abs/2010.11929> (arXiv:2010.11929 [cs])
- Dowell, D. C., Alexander, C. R., James, E. P., Weygandt, S. S., Benjamin, S. G., Manikin, G. S., ... Alcott, T. I. (2022, August). The High-Resolution Rapid Refresh (HRRR): An Hourly Updating Convection-Allowing Forecast Model. Part I: Motivation and System Description. *Weather and Forecasting*, 37(8), 1371–1395. Retrieved 2024-09-28, from <https://journals.ametsoc.org/view/journals/wefo/37/8/WAF-D-21-0151.1.xml> doi: 10.1175/WAF-D-21-0151.1
- ECMWF. (2022, May). *Integrated Forecasting System* [Text]. Retrieved 2024-09-28, from <https://www.ecmwf.int/en/forecasts/documentation-and-support/changes-ecmwf-model>
- Gilmer, J., Schoenholz, S. S., Riley, P. F., Vinyals, O., & Dahl, G. E. (2017, June). *Neural Message Passing for Quantum Chemistry*. arXiv. Retrieved 2024-09-25, from <http://arxiv.org/abs/1704.01212> (arXiv:1704.01212 [cs]) doi: 10.48550/arXiv.1704.01212
- Giorgi, F., Coppola, E., Solmon, F., Mariotti, L., Sylla, M. B., Bi, X., ... Brankovic, C. (2012, March). RegCM4: model description and preliminary tests over

- multiple CORDEX domains. *Climate Research*, 52, 7–29. Retrieved 2025-03-06, from <https://www.int-res.com/abstracts/cr/v52/p7-29/> doi: 10.3354/cr01018
- Harder, P., Hernandez-Garcia, A., Ramesh, V., Yang, Q., Sattigeri, P., Szwarcman, D., ... Rolnick, D. (2023). Hard-Constrained Deep Learning for Climate Downscaling. *Journal of Machine Learning Research*, 24(365), 1–40. Retrieved 2024-10-01, from <http://jmlr.org/papers/v24/23-0158.html>
- Hernanz, A., García-Valero, J. A., Domínguez, M., Ramos-Calzado, P., Pastor-Saavedra, M. A., & Rodríguez-Camino, E. (2022). Evaluation of statistical downscaling methods for climate change projections over Spain: Present conditions with perfect predictors. *International Journal of Climatology*, 42(2), 762–776. Retrieved 2025-03-06, from <https://onlinelibrary.wiley.com/doi/abs/10.1002/joc.7271> (_eprint: <https://onlinelibrary.wiley.com/doi/pdf/10.1002/joc.7271>) doi: 10.1002/joc.7271
- Hersbach, H., Bell, B., Berrisford, P., Hirahara, S., Horányi, A., Muñoz-Sabater, J., ... Thépaut, J.-N. (2020). The ERA5 global reanalysis. *Quarterly Journal of the Royal Meteorological Society*, 146(730), 1999–2049. Retrieved 2024-09-23, from <https://onlinelibrary.wiley.com/doi/abs/10.1002/qj.3803> (_eprint: <https://onlinelibrary.wiley.com/doi/pdf/10.1002/qj.3803>) doi: 10.1002/qj.3803
- Kochkov, D., Yuval, J., Langmore, I., Norgaard, P., Smith, J., Mooers, G., ... Hoyer, S. (2024, July). Neural general circulation models for weather and climate. *Nature*. Retrieved 2024-07-23, from <https://www.nature.com/articles/s41586-024-07744-y> doi: 10.1038/s41586-024-07744-y
- Lam, R., Sanchez-Gonzalez, A., Willson, M., Wirsberger, P., Fortunato, M., Alet, F., ... Battaglia, P. (2023, December). Learning skillful medium-range global weather forecasting. *Science*, 382(6677), 1416–1421. Retrieved 2024-03-09, from <https://www.science.org/doi/10.1126/science.adi2336> doi: 10.1126/science.adi2336
- Lang, S., Alexe, M., Chantry, M., Dramsch, J., Pinault, F., Raoult, B., ... Rabier, F. (2024, June). *AIFS - ECMWF's data-driven forecasting system*. arXiv. Retrieved 2024-06-19, from <http://arxiv.org/abs/2406.01465> (arXiv:2406.01465 [physics])
- Lessig, C., Luise, I., Gong, B., Langguth, M., Stadler, S., & Schultz, M. (2023, September). *AtmoRep: A stochastic model of atmosphere dynamics using large scale representation learning*. arXiv. Retrieved 2024-03-09, from <http://arxiv.org/abs/2308.13280> (arXiv:2308.13280 [physics])
- Mouatadid, S., Orenstein, P., Flaspohler, G., Cohen, J., Oprescu, M., Fraenkel, E., & Mackey, L. (2023, June). Adaptive bias correction for improved subseasonal forecasting. *Nature Communications*, 14(1), 3482. Retrieved 2024-11-18, from <https://www.nature.com/articles/s41467-023-38874-y> doi: 10.1038/s41467-023-38874-y
- Nguyen, T., Brandstetter, J., Kapoor, A., Gupta, J. K., & Grover, A. (2023, December). *ClimaX: A foundation model for weather and climate*. arXiv. Retrieved 2024-03-09, from <http://arxiv.org/abs/2301.10343> (arXiv:2301.10343 [cs])
- Oskarsson, J., Landelius, T., & Lindsten, F. (2023, November). *Graph-based Neural Weather Prediction for Limited Area Modeling*. arXiv. Retrieved 2024-06-03, from <http://arxiv.org/abs/2309.17370> (arXiv:2309.17370 [cs, stat])
- Pathak, J., Subramanian, S., Harrington, P., Raja, S., Chattopadhyay, A., Mardani, M., ... Anandkumar, A. (2022, February). *FourCastNet: A Global Data-driven High-resolution Weather Model using Adaptive Fourier Neural Operators*. arXiv. Retrieved 2024-04-15, from <http://arxiv.org/abs/2202.11214> (arXiv:2202.11214 [physics])

- Pfaff, T., Fortunato, M., Sanchez-Gonzalez, A., & Battaglia, P. W. (2021, June). *Learning Mesh-Based Simulation with Graph Networks*. arXiv. Retrieved 2024-07-23, from <http://arxiv.org/abs/2010.03409> (arXiv:2010.03409 [cs])
- Prasad, A., Harder, P., Yang, Q., Sattegeri, P., Szwarcman, D., Watson, C., & Rolnick, D. (2024, July). *Evaluating the transferability potential of deep learning models for climate downscaling*. arXiv. Retrieved 2024-10-01, from <http://arxiv.org/abs/2407.12517> (arXiv:2407.12517 [cs]) doi: 10.48550/arXiv.2407.12517
- Ramavajjala, V., & Mitra, P. P. (2023, September). *Verification against in-situ observations for Data-Driven Weather Prediction*. arXiv. Retrieved 2024-01-22, from <http://arxiv.org/abs/2305.00048> (arXiv:2305.00048 [physics]) doi: 10.48550/arXiv.2305.00048
- Ronneberger, O., Fischer, P., & Brox, T. (2015, May). *U-Net: Convolutional Networks for Biomedical Image Segmentation*. arXiv. Retrieved 2024-09-24, from <http://arxiv.org/abs/1505.04597> (arXiv:1505.04597 [cs]) doi: 10.48550/arXiv.1505.04597
- Sanchez-Gonzalez, A., Godwin, J., Pfaff, T., Ying, R., Leskovec, J., & Battaglia, P. W. (2020, September). *Learning to Simulate Complex Physics with Graph Networks*. arXiv. Retrieved 2024-09-24, from <http://arxiv.org/abs/2002.09405> (arXiv:2002.09405 [physics, stat]) doi: 10.48550/arXiv.2002.09405
- Schmude, J., Roy, S., Trojak, W., Jakubik, J., Civitarese, D. S., Singh, S., ... Ramachandran, R. (2024, September). *Prithvi WxC: Foundation Model for Weather and Climate*. arXiv. Retrieved 2024-09-24, from <http://arxiv.org/abs/2409.13598> (arXiv:2409.13598 [physics])
- Skamarock, W., Klemp, J., Dudhia, J., Gill, D. O., Barker, A. D., Duda, M. G., ... Powers, J. G. (2008). *A Description of the Advanced Research WRF Version 3* (Tech. Rep.). Retrieved 2025-03-06, from <https://opensky.ucar.edu/islandora/object/technotes%3A500>
- Stengel, K., Glaws, A., Hettinger, D., & King, R. N. (2020, July). Adversarial super-resolution of climatological wind and solar data. *Proceedings of the National Academy of Sciences*, 117(29), 16805–16815. Retrieved 2025-03-06, from <https://www.pnas.org/doi/10.1073/pnas.1918964117> (Publisher: Proceedings of the National Academy of Sciences) doi: 10.1073/pnas.1918964117
- Storch, H. v., Zorita, E., & Cubasch, U. (1993, June). Downscaling of Global Climate Change Estimates to Regional Scales: An Application to Iberian Rainfall in Wintertime. *Journal of Climate*. Retrieved 2025-03-06, from https://journals.ametsoc.org/view/journals/clim/6/6/1520-0442_1993_006_1161_dogcce_2_0_co_2.xml (Section: Journal of Climate)
- Vandal, T., Kodra, E., Ganguly, S., Michaelis, A., Nemani, R., & Ganguly, A. R. (2017, March). *DeepSD: Generating High Resolution Climate Change Projections through Single Image Super-Resolution*. arXiv. Retrieved 2025-03-06, from <http://arxiv.org/abs/1703.03126> (arXiv:1703.03126 [cs]) doi: 10.48550/arXiv.1703.03126
- Vaswani, A., Shazeer, N., Parmar, N., Uszkoreit, J., Jones, L., Gomez, A. N., ... Polosukhin, I. (2023, August). *Attention Is All You Need*. arXiv. Retrieved 2023-11-03, from <http://arxiv.org/abs/1706.03762> (arXiv:1706.03762 [cs])
- Vaughan, A., Markou, S., Tebbutt, W., Requeima, J., Bruinsma, W. P., Andersson, T. R., ... Turner, R. E. (2024, July). *Aardvark weather: end-to-end data-driven weather forecasting*. arXiv. Retrieved 2025-04-25, from <http://arxiv.org/abs/2404.00411> (arXiv:2404.00411 [physics]) doi: 10.48550/arXiv.2404.00411
- Wilby, R. L. (1998, December). Statistical downscaling of daily precipitation using daily airflow and seasonal teleconnection indices. *Climate Research*, 10(3),

- 163–178. Retrieved 2025-03-06, from <https://www.int-res.com/abstracts/cr/v10/n3/p163-178/> doi: 10.3354/cr010163
- Yang, Q., Hernandez-Garcia, A., Harder, P., Ramesh, V., Sattegeri, P., Szwarcman, D., ... Rolnick, D. (2023, May). *Fourier Neural Operators for Arbitrary Resolution Climate Data Downscaling*. arXiv. Retrieved 2024-10-01, from <http://arxiv.org/abs/2305.14452> (arXiv:2305.14452 [physics]) doi: 10.48550/arXiv.2305.14452
- Zorita, E., & Storch, H. v. (1999, August). The Analog Method as a Simple Statistical Downscaling Technique: Comparison with More Complicated Methods. *Journal of Climate*. Retrieved 2025-03-06, from https://journals.ametsoc.org/view/journals/clim/12/8/1520-0442_1999_012_2474_tamaas_2.0.co_2.xml (Section: Journal of Climate)

Appendix A

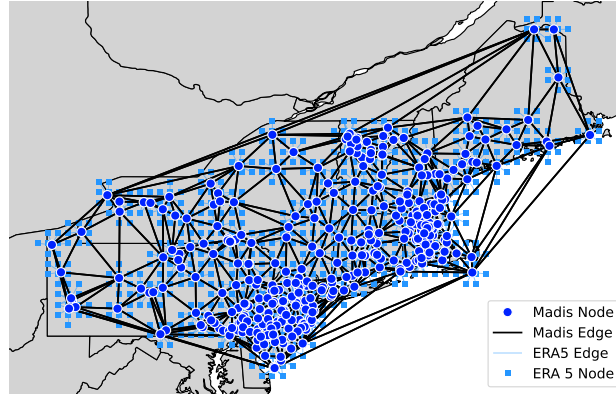


Figure A1. Weather station and ERA5 graph for the US Northeast study region. MADIS stations are shown as dark blue circles; the black edges connect each weather station in a Delaunay Network. ERA5 nodes are shown as light blue squares, and each weather station is connected to its 8 nearest ERA5 neighbors.

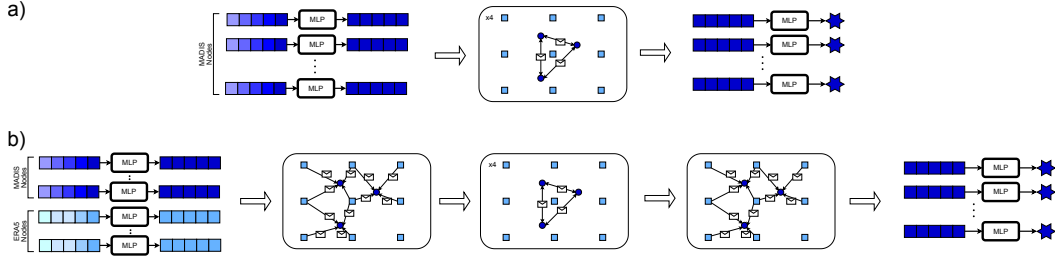


Figure A2. MPNN model architecture. (a) MPNN model architecture without ERA5. Time series of weather variables at MADIS stations are embedded with an MLP. These node embeddings are updated with four iterations of message passing according to a pre-defined graph of MADIS stations. The final node embeddings are decoded with another MLP to generate forecasts at each MADIS station. (b) MPNN model architecture with ERA5. Time series of weather variables at MADIS stations and ERA5 grids are embedded with two separate MLPs. MADIS node embeddings are first updated with messages coming from neighboring ERA5 nodes. They are then iteratively updated four times based on a MADIS station graph (the same graph as (a)). The node embeddings are lastly updated with neighboring ERA5 nodes again; are finally decoded as forecasts by an MLP.

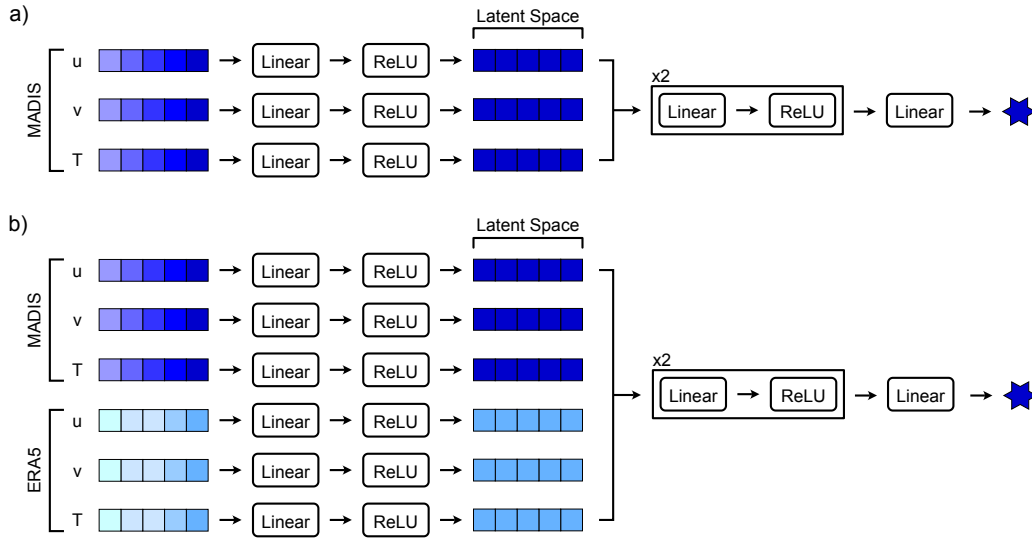


Figure A3. MLP model architecture. (a) MLP model architecture without ERA5 input. Time series of weather variables at a MADIS station are embedded with a linear layer. The embedded features are processed by two linear layers, and finally decoded with another linear layer as prediction. (b) MLP model architecture with ERA5 input. It follows a similar architecture to (a) but with additional inputs of interpolated ERA5 to a MADIS station.

Table A1. Summary of our curated dataset. This consists of three parts: ERA5, HRRR, and MADIS.

Name	Type	Temporal Span	Spatial Span	Variables
ERA5	Gridded Mesh	2019–2023	Northeast US	10m u , 10m v , 2m temperature, 2m dewpoint temperature,
HRRR	Gridded Mesh	2019–2023	Northeast US	10m u , 10m v , 2m temperature, 2m dewpoint temperature,
MADIS	Off-Grid Station	2019–2023	Northeast US	10m wind speed, 10m wind direction, 2m temperature, 2m dewpoint temperature,

Table A2. Test set Wind Vector Error of experiments for each lead time. Wind Vector Error is averaged over stations and time steps for the year 2023.

Model	ExternalDataset	1	2	4	8	12	18	24	36	48	Mean Error
Interpolation	ERA5	2.6206	2.6206	2.6206	2.6206	2.6206	2.6206	2.6206	2.6206	2.6206	2.6206
Interpolation	HRRR-R	2.4617	2.4617	2.4617	2.4617	2.4617	2.4617	2.4617	2.4617	2.4617	2.4617
Interpolation	HRRR-F	2.6235	2.6506	2.6659	2.6901	2.7177	2.7792	-	-	-	2.6880
Persistence	-	0.3885	0.5165	0.6953	0.9373	1.0740	1.1415	1.1464	1.3364	1.2522	0.9431
MLP	-	0.3855	0.5012	0.6500	0.8090	0.8683	0.8943	0.9053	0.9261	0.9262	0.7629
MLP	ERA5	0.4474	0.5366	0.6267	0.6930	0.6956	0.6844	0.6997	0.7136	0.7370	0.6482
MLP	HRRR-F	0.4252	0.5294	0.6228	0.6970	0.7247	0.7244	0.8399	0.9255	0.9265	0.7128
MLP	HRRR-R	0.4391	0.5229	0.6105	0.6721	0.6509	0.6667	0.6624	0.6729	0.6857	0.6204
GNN	-	0.4290	0.5235	0.6518	0.7806	0.8487	0.8821	0.9009	0.9258	0.9300	0.7636
GNN	ERA5	0.4201	0.5146	0.6097	0.6991	0.7159	0.6941	0.7079	0.7248	0.7148	0.6446
GNN	HRRR-F	0.4171	0.5089	0.6123	0.6957	0.6991	0.7133	0.8482	0.9119	0.9288	0.7039
GNN	HRRR-R	0.4248	0.5015	0.5969	0.6721	0.7030	0.6661	0.6700	0.6849	0.6886	0.6231
Transformer	-	0.3782	0.4838	0.6040	0.7216	0.7791	0.8515	0.8867	0.9113	0.9123	0.7254
Transformer	ERA5	0.3736	0.4444	0.5081	0.5185	0.5284	0.5260	0.5354	0.5388	0.5351	0.5009
Transformer	HRRR-F	0.3791	0.4458	0.4943	0.5335	0.5464	0.5617	0.7019	0.8713	0.9130	0.6052
Transformer	HRRR-R	0.3759	0.4364	0.4819	0.4948	0.5041	0.5086	0.5055	0.5160	0.5224	0.4828

Table A3. Test set Temperature RMSE of experiments for each lead time. Temperature RMSE is averaged over stations and time steps for the year 2023.

Model	ExternalDataset	1	2	4	8	12	18	24	36	48	Mean Error
Interpolation	ERA5	2.0285	2.0285	2.0285	2.0285	2.0285	2.0285	2.0285	2.0285	2.0285	2.0285
Interpolation	HRRR-R	1.6824	1.6824	1.6824	1.6824	1.6824	1.6824	1.6824	1.6824	1.6824	1.6824
Interpolation	HRRR-F	1.7706	1.8379	1.9356	2.0467	2.1033	2.1501	-	-	-	1.9740
Persistence	-	1.1285	2.0531	3.5960	5.6626	6.4681	5.6292	4.3057	7.3789	5.3896	4.6235
MLP	-	0.8586	1.3821	2.1692	3.0583	3.4384	3.7497	3.9832	4.6830	4.8350	3.1286
MLP	ERA5	1.6848	1.7721	2.1847	2.6728	2.6778	2.5402	2.5701	2.5190	2.2849	2.3229
MLP	HRRR-F	1.5682	2.2566	2.1774	2.8183	2.7663	2.9323	3.0804	3.5388	4.2048	2.8159
MLP	HRRR-R	1.5194	1.9444	2.0540	2.4136	2.6902	2.0723	2.1444	2.0465	2.3971	2.1424
GNN	-	1.6763	2.0039	2.4243	2.8027	3.3179	3.3818	3.9041	4.4925	5.0684	3.2302
GNN	ERA5	1.7567	2.0910	2.2112	2.7139	2.8009	2.3816	2.5855	2.8181	2.2044	2.3959
GNN	HRRR-F	1.7773	1.8839	2.8742	2.5763	2.8597	2.7491	3.0851	3.6259	4.1813	2.8459
GNN	HRRR-R	1.7077	1.9705	2.0594	2.4264	2.7071	2.6259	3.0305	2.8871	2.4290	2.4271
Transformer	-	0.8453	1.3104	1.9738	2.6415	2.9751	3.3225	3.6866	4.3659	4.5679	2.8543
Transformer	ERA5	0.7850	1.1293	1.4047	1.5725	1.5897	1.5775	1.6328	1.6226	1.6761	1.4434
Transformer	HRRR-F	0.7890	1.1146	1.4106	1.6805	1.7700	1.8012	2.4541	3.3228	4.1414	2.0538
Transformer	HRRR-R	0.7709	0.9916	1.2261	1.3163	1.3852	1.3612	1.3775	1.4410	1.4685	1.2598

Table A4. Test set Dewpoint RMSE of experiments for each lead time. Dewpoint RMSE is averaged over stations and time steps for the year 2023.

Model	ExternalDataset	1	2	4	8	12	18	24	36	48	Mean Error
Interpolation	ERA5	3.5549	3.5549	3.5549	3.5549	3.5549	3.5549	3.5549	3.5549	3.5549	3.5549
Interpolation	HRRR-R	3.4996	3.4996	3.4996	3.4996	3.4996	3.4996	3.4996	3.4996	3.4996	3.4996
Interpolation	HRRR-F	3.5716	3.5926	3.6243	3.6774	3.7137	3.7326	-	-	-	3.6520
Persistence	-	0.7834	1.2740	2.0021	3.0099	3.6988	4.3591	4.8231	5.8531	6.1053	3.5454
MLP	-	0.7919	1.2483	1.8765	2.7753	3.3775	3.9771	4.3993	5.0861	5.3832	3.2128
MLP	ERA5	1.4267	1.6521	1.9811	2.5329	2.9191	2.7480	2.8060	2.7717	2.5846	2.3802
MLP	HRRR-F	1.4384	2.0339	2.0095	2.5592	2.7156	2.8836	2.9783	3.6511	4.5118	2.7535
MLP	HRRR-R	1.3789	1.6538	2.0259	2.4997	2.7184	2.4792	2.4657	2.4913	2.7995	2.2792
GNN	-	1.4278	1.8289	2.0423	2.5904	2.9936	3.4755	3.9815	4.8123	5.3336	3.1651
GNN	ERA5	1.4616	1.7783	2.2188	2.4419	2.7946	2.6365	2.8001	3.0051	2.4818	2.4021
GNN	HRRR-F	1.4717	1.8274	2.6824	2.3998	3.0036	2.7710	3.0227	3.7669	4.4572	2.8225
GNN	HRRR-R	1.7071	1.6215	1.9472	2.4414	2.7491	2.6551	3.0125	2.9933	2.6584	2.4206
Transformer	-	0.7721	1.1771	1.7359	2.3718	2.6763	3.4317	3.9042	4.7105	5.0570	2.8707
Transformer	ERA5	0.7820	1.1003	1.3715	1.6132	1.6945	1.7553	1.8099	1.8821	1.9115	1.5467
Transformer	HRRR-F	0.7566	1.1658	1.3903	1.6845	1.8506	1.9727	2.4297	3.5142	4.4056	2.1300
Transformer	HRRR-R	0.7634	1.0256	1.3041	1.4809	1.6162	1.6522	1.7129	1.7841	1.8297	1.4632

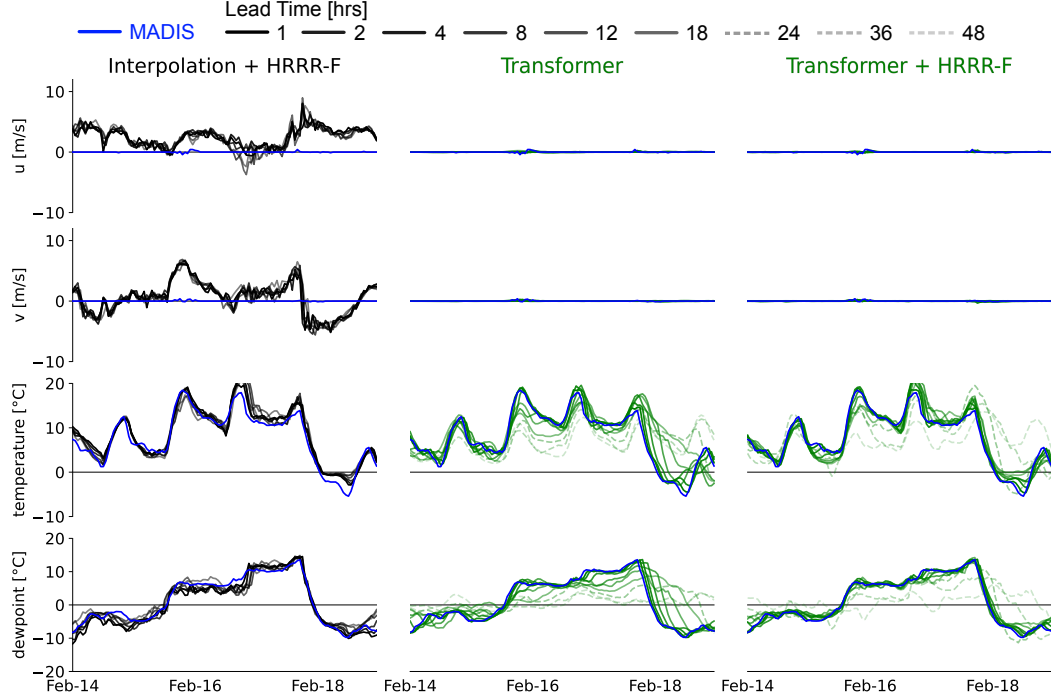


Figure A4. Example time series from one weather station where transformer + HRRR-F shows the smallest error. From top to bottom: time series of 10m u and v components, 2m temperature, and 2m dewpoint are presented. Each panel has the MADIS ground truth in blue, and the predictions at increasing lead times displayed with decreasing saturation. For this station and time snippet the interpolated HRRR-F appears rather inaccurate for wind vector estimation. The wind vector value is very close to zero suggesting wind blocking effect from local topography, which is extremely hard to be captured by large-scale numerical model like HRRR. By ingesting history of local measurements, the transformer is able to easily capture this local heterogeneity.

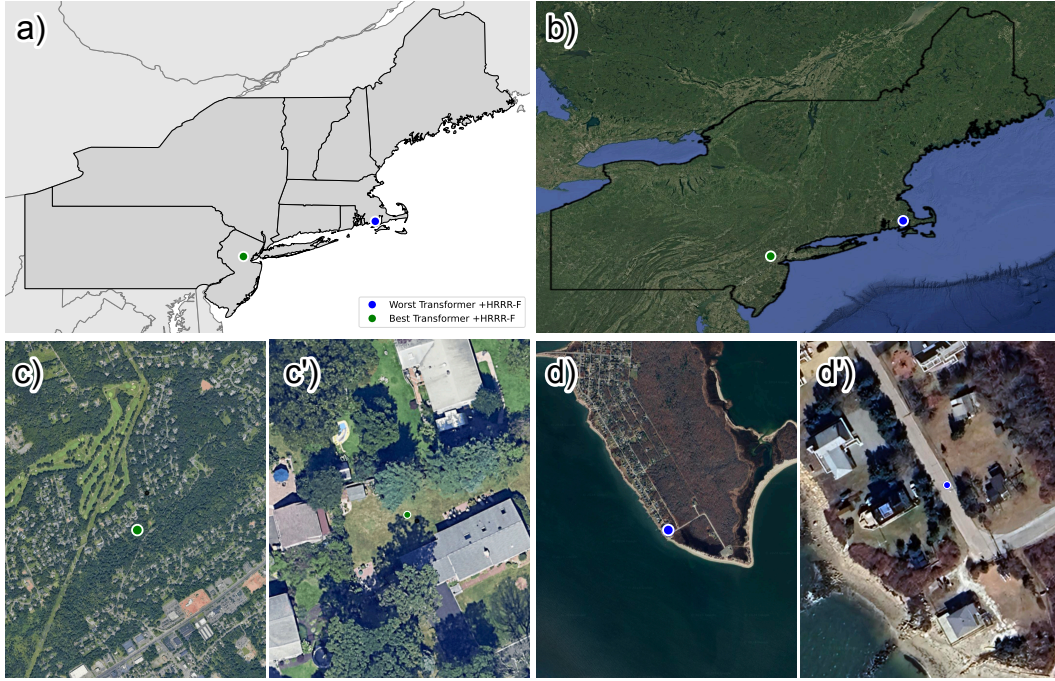


Figure A5. Examples of environments for two selected weather stations. (a) Overview of the two stations. (b) Google Satellite image of the two selected weather stations. The two selected weather stations are: (c) the station with the best overall Transformer + HRRR-F loss, (d) and the station with the worst overall Transformer + HRRR-F loss. (c) and (d) show a zoomed-out view of each area; (c') and (d') are zoomed in. (c) shows good examples of weather stations being surrounded by trees and buildings, where wind is affected by these local surface characteristics.